# Land surface temperature from satellite data *

H. GRASSL

*GKSS-Forschungszentrum Geesthacht GmbH, Geesthacht, Federal Republic of Germany*

**Summary**

A short section on theory of remote sensing by electromagnetic waves in the visible and infrared part of the spectrum, and an account of surface parameters, gases and aerosol particle characteristics influencing the remote measurement of surface temperature are given. Algorithms to establish a stand-alone remote surface temperature measurement are shown. Finally a variety of applications of different algorithms also including the daily temperature amplitude determination is discussed.

## 1. Introduction

All fluxes determining the energy budget of a surface element, except solar radiation flux, involve — if parameterized — surface temperature either directly like longwave net flux or indirectly via a temperature gradient like sensible heat flux and latent heat flux into the atmosphere as well as the sensible heat flux into the soil. Therefore the twodimensional surface temperature distribution is needed, whenever the total energy budget or parts of it are sought for any area. Since the direct measurement of surface skin temperature is impossible (due to the disturbance by any thermometer) an ideal means is the radiometric determination of temperature via surface emission within the thermal infrared spectrum from an airplane or a satellite.

Immediately two error sources come into play:
— the non-blackness of all natural surfaces;
— the emission of the atmosphere between the measuring platform and the surface, at temperatures differing from surface temperature.

---

* This paper is a revised version of a lecture given within a course on «Application of Remote Sensing to Agrometeorology» at Ispra, April 1987.

Both errors vary with time for a distinct surface element in both cases mainly caused by changes in water content either by a change from a dry to a wet surface or by changes in atmospheric water vapour.

Since the atmosphere has no perfect spectral window in the thermal infrared a one channel radiometer for the remote measurement of surface temperature may at best apply a climatological mean correction of the atmosphere's masking, if no calibration points are available.

This lecture will give — after a short section on theory — an account of surface parameters, gases and aerosol particle characteristics influencing the remote measurement of surface temperature, will then show algorithms to establish a stand-alone remote surface temperature measurement, and will finally discuss a variety of applications of different algorithms also including the daily temperature amplitude determination.

## 2. Necessary physical background

### 2.1 Governing equations

Remote sensing by electromagnetic waves in the visible and infrared part of the spectrum normally applies time averages over many waves. The appropriate equation governing the time averaged squares of amplitudes of electromagnetic waves is the radiative transfer equation.

Written for spectral radiance $I_\lambda$, the energy flowing through unit surface from a unit space angle per unit time and unit spectral interval (here wavelength $\lambda$; thus the dimension is $Wm^{-2}\ sr^{-1}\ \mu m^{-1}$)

$$\frac{dI_\lambda}{d\tau_\lambda} = -I_\lambda + J_\lambda \qquad\qquad \text{or}$$

$$\frac{dI_\lambda}{ds} = (-I_\lambda + J_\lambda) \cdot e_\lambda \qquad\qquad (1)$$

it simply states that firstly the incoming spectral radiance $I_\lambda$ is the stronger reduced the stronger the spectral optical depth increment $d\tau_\lambda$ of a medium is, and that secondly $I_\lambda$ may be increased by a source $J_\lambda$. The spectral optical depth $\tau_\lambda$ is here defined as the integral over spectral volume extinction coefficient $e_\lambda$ along a distinct direction $s$

$$\tau_\lambda = \int_0^{s^*} e_\lambda\ ds \qquad\qquad (2)$$

For thermal infrared remote sensing the integration of equation (1) (an integro-differential equation in scattering media) may be simplified strongly by neglecting scattering in the atmosphere thus reducing the spectral source $J_\lambda$ to Planck's function $B_\lambda$, which merely depends on temperature T. This simplification is a good approximation for all cloudless areas in the thermal infrared outside very strong atmospheric turbidity layers. As a rule of thumb the scattering optical depth caused by aerosols is by a factor of 5 smaller in the main thermal infrared window from 10-13 µm wavelength as compared to the visible wavelength, where $\tau_{aerosol} < 0.2$ is mostly fulfilled.

After a formal integration along a distinct path in a non-scattering atmosphere, here from $\tau_\lambda = 0$ at the top of the atmosphere — where as a boundary condition no emission from space is assumed, i.e. $I_\lambda^- = 0$ — to the ground with total optical depth $\tau_\lambda^*$, we get for the spectral radiance $I_\lambda^+$ emerging at the top of the atmosphere

$$I_\lambda^+ = \varepsilon_\lambda \ B_\lambda \ (T_s) \ e^{-\tau_\lambda} \qquad\qquad \text{surface} \qquad\qquad (3)$$
surface
contribution

$$+ \int_0^{\tau_\lambda^*} B_\lambda \ T \ (\tau_\lambda) \ e^{-\tau_\lambda} d\tau_\lambda \qquad\qquad \text{atmospheric}$$
atmospheric
emission

$$+ (1 - \varepsilon_\lambda) \ (\int_{\tau_\lambda^*}^0 B_\lambda \ (T(\tau_\lambda)) \ e^{-\tau_\lambda} \ d\tau_\lambda) \ e^{-\tau_\lambda^*}$$
surface reflection of downwelling emission of the atmosphere (here written for a smooth surface only)

Only the first term on the right side contains information on surface temperature $T_s$ via Planck's function $B_\lambda(T_s)$; ideally the spectral emissivity $\varepsilon_\lambda$ reaches unity for a blackbody. Fortunately, most natural surfaces, especially water and vegetated surfaces, reach $\varepsilon_\lambda > 0.95$, even $\varepsilon_\lambda \simeq 0.99$ in thermal infrared windows. In order to get the spectral surface emission $\varepsilon_\lambda B_\lambda(T_s)$ to the satellite the spectral transmission $t_\lambda = e^{-\tau_\lambda}$ of the atmosphere should be as small as possible, i.e. only atmospheric windows are suitable wavelength positions.

The second term, atmospheric emission, masks the surface contribution.

If near surface layers of the atmosphere with $B_\lambda(T(\tau_\lambda))$ only slightly smaller than $B_\lambda(T_s)$ constitute the main part of the integral of the second term, the transmission loss of surface emission in term number one is to a big part compensated. However, this is not at all the case for high aerosol particle layers or subvisible cirrus clouds both emitting at low temperatures. In this case even very small spectral optical depth values with $\tau_\lambda \leq 0.01$ may cause

up to one percent error in spectral upward radiance $I_\lambda^+$, which at ambient temperatures of 20°C is approximately equivalent to a one degree temperature error if measuring in the 10-13 µm central infrared window. Since vertical temperature and humidity structure (water vapour absorption is the dominant absorption in the windows) vary strongly depending on weather condition and geographical position the above mentioned degree of compensation also varies, leaving a variety of necessary corrections for the atmosphere's masking ranging from no correction to up to 10 K.

The third term accounts for the reflection of downwelling thermal infrared radiances by the surface. Its importance decreases with increasing $\varepsilon_\lambda$ and extinction by the atmosphere, thus it is nearly negligible over water surfaces in the tropics and it becomes important in moderately humid atmospheres over rock surfaces. If handled accurately for a rough surface, either composed of surface elements with different slopes or vegetated this term needs a proper description of spectral emissivity $\varepsilon_\lambda$ as a function of both the angle of incidence of downwelling radiance and the surface element slope distribution. Its effect is a partial compensation of the blackbody emissivity deficit in term number one, with growing compensation for increasing surface roughness.

## 2.2 *Relation to temperature*

The quantity desired is surface temperature $T_s$ and it is hidden in spectral Planck's function $B_\lambda(T_s)$. Any upwelling spectral radiance $I_\lambda^+$, the satellite signal, may be expressed in a so called brightness temperature $T_B$, which merely is a temperature a blackbody emitting the same spectral radiance would have. The simple inversion of Planck's law

$$B_\lambda\,(T)\ d_\lambda = \frac{2hc^2}{\lambda^5}\cdot\frac{1}{e^{hc/\lambda T}-1}\ d\lambda \qquad\qquad (4a)$$

$$B_v\,(T)\ d_v = \frac{2hv^3}{c^2}\cdot\frac{1}{e^{vh/kT}-1}\ d\lambda \qquad (4b)$$

(4b) (if written for wavenumber $v = 1/\lambda$ in spectroscopy)

(h = Planck's constant, c = velocity of light, k = Boltzmann's constant)

gives brightness temperature $T_B$

$$T_B = \frac{a}{\ln B_v(T) - b}\ ;\quad a = c_2\,v;\quad b = \ln c_1\,v^3;\quad c_1 = 2h/c^2;\quad c_2 = h/k \qquad (5)$$

It is generally accepted to convert satellite signals $I_\lambda^+$ into brightness temperatures $T_B$. However, these values erroneously are often used directly as surface temperatures before the atmospheric masking has been corrected. Before these corrections will be introduced equation (3) and also equation (5), which where written for the monochromatic idealization, have to be adapted to the finite spectral width of a radiometer channel.

## 2.3 Account of the finite spectral width

The width of satellite radiometer channels causes a modification of the idealized equations (3) and (5). If the normalized spectral transmission $\varphi^*(v)$ or $\varphi^*(\lambda)$, for which we have

$$\int_{v_1}^{v_2} \varphi^* (v) \, dv = \int_{\lambda_1}^{\lambda_2} \varphi^* (\lambda) \, d\lambda = 1, \tag{6}$$

is introduced into equation (3) the real satellite signal becomes

(7)

$$I_{\Delta v}^+ = \int_{v_1}^{v_2} I_v^+ \cdot \varphi^* (v) \, dv \qquad \text{with } v_1, v_2 = \text{wavenumber for which } \varphi^* (v) = 0 \text{ if } v < v_1 \text{ and } v > v_2$$

$$= \int_{v_1}^{v_2} B_v (T_B) \cdot \varphi^* (v) \, dv$$

$$I_{\Delta\lambda}^+ = \int_{\lambda_1}^{\lambda_2} I_\lambda^+ \cdot \varphi^* (\lambda) \, d\lambda \qquad \text{with } \lambda_1, \lambda_2 = \text{wavelength for which } \varphi^*(\lambda) = 0 \text{ if } \lambda < \lambda_1 \text{ and } \lambda > \lambda_2$$

$$= \int_{\lambda_1}^{\lambda_2} B_\lambda(T_B) \cdot \varphi^*(\lambda) d\lambda$$

Since $\varphi^*(v)$ is not simply to be expressed by an analytical function, equation (7) cannot exactly be — as equation (5) — converted into a brightness temperature $T_B$. Following an empirical approach by Singh (1984) the brightness temperature $T_B$ of existing satellite radiometer channels is sufficiently accurate if described by

$$T_B = a_1 + b_1 \cdot T_B' \tag{8}$$

where the so called preliminary brightness temperature $T_B'$ is related to $I_{\Delta\nu}^+$ as follows

$$T_B' = \frac{b_2}{\ln I_{\Delta\nu}^+ - a_2} \qquad \text{(equivalent to equation (5))} \qquad (9)$$

This approach also accounts — in equation (8) — for eventually occurring non-linear calibration curves of a satellite radiometer.

As an example Table 1 displays the coefficients for all three thermal infrared channels with central wavelengths $\bar{\lambda}$ at 3.7, 11, and 12 μm of the NOAA 7 polar orbiting satellite, the first to contain the split-window at 11 and 12 μm.

TABLE 1 - *Coefficients in equations (8) and (9) needed for the determination of $T_B$ for the Advanced Very High Resolution Radiometer (AVHRR) infrared channels onboard NOAA 7 satellite*

| Channel | $\bar{\lambda}$ | $a_1 K$ | $b_1$ | $a_2$ | $b_2 K$ |
|---------|-----------------|---------|-------|-------|---------|
| 3 | 3.7 μm | 0 | 1 | 12.2554 | −3821.046 |
| 4 | 11 μm | −12.920 | 1.045 | 9.2058 | −1344.832 |
| 5 | 12 μm | − 7.717 | 1.027 | 8.9373 | −1226.189 |

## 2.4 ΔT for different atmospheres

The dependence of the temperature correction $\Delta T$ on different situations is best explained by showing $\Delta T$ for variations of spectral emissivity $\varepsilon_\lambda$, water vapour content, temperature structure, viewing angle, aerosol particle optical depth and optically thin, not detected clouds.

The best way to get an overview of possible corrections is by numerical simulations with a radiative transfer model. The following results were all available before a procedure for land surface temperature determination has been devised.

### 2.4.1 Emissivity dependence

Within the $0.95 < \varepsilon_{\Delta\lambda} < 1.0$ range of mean surface emissivity $\varepsilon_{\Delta\lambda}$ for the wavelength band $\Delta\lambda$ of a radiometer channel the temperature correction $\Delta T$, used to infer surface temperature $T_s$ by

$$T_S = T_B + \Delta T \qquad (10)$$

is nearly linearly depending on the deviation from the blackbody emission $1 - \varepsilon_{\Delta\lambda}$ with $\Delta T/\Delta\varepsilon_{\Delta\lambda} = -0.45$ K for a one percent change in mean emissivity $\varepsilon_{\Delta\lambda}$. Moreover, $\Delta T/\Delta \varepsilon_{\Delta\lambda}$ is only slightly dependent on temperature structure close to the ground and on spectral position within the main thermal infrared window (Fig. 1).

### 2.4.2. *Water vapour influence*

Water vapour is the dominant absorber within the thermal infrared window from 10-13 μm wavelength. There is no possibility to reduce its influen-
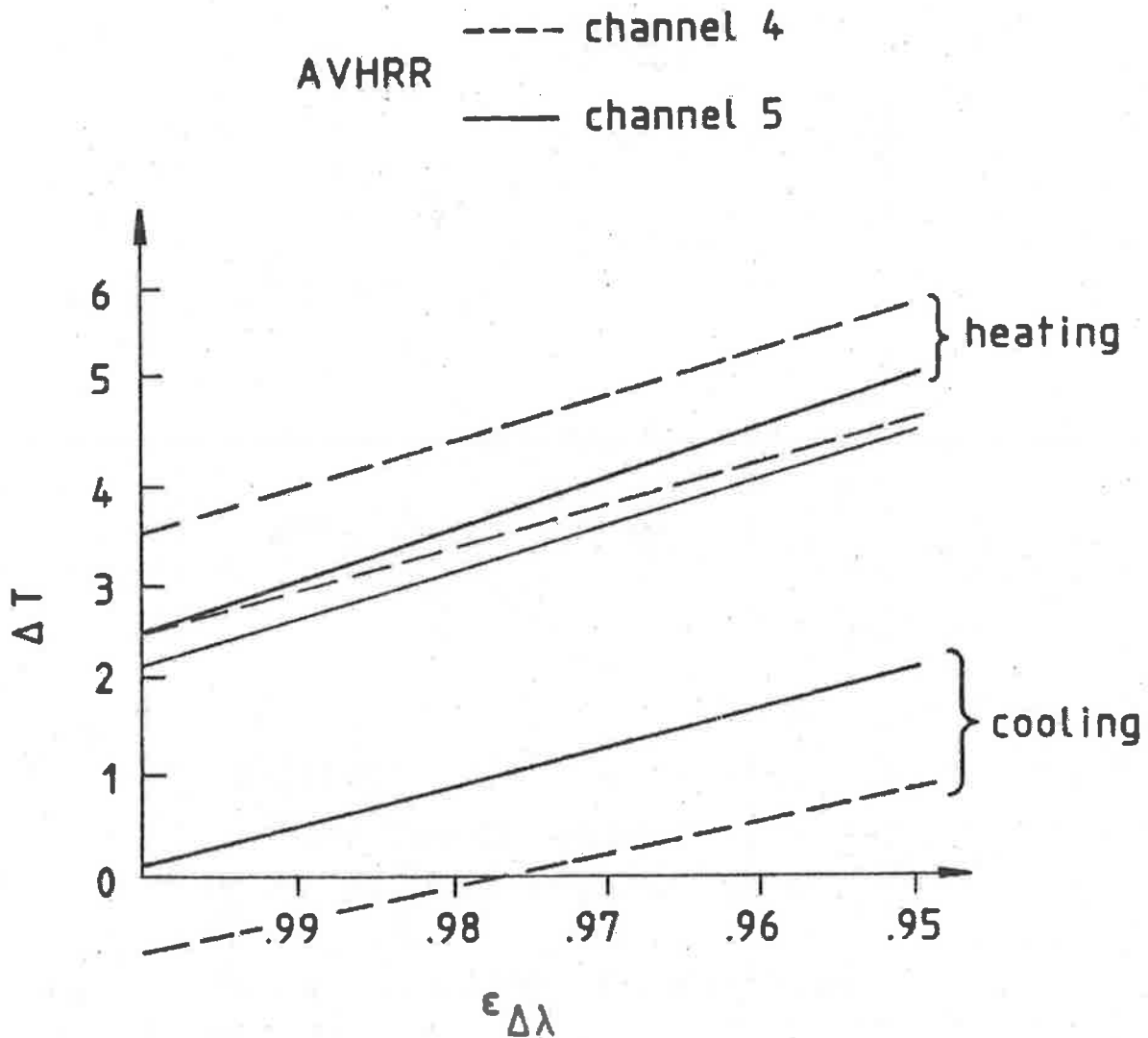


Figure 1 - *Temperature correction $\Delta T$ in a 45 °N standard atmosphere as a function of mean spectral surface emissivity $\varepsilon_{\Delta\lambda}$ for the wavelength band of a radiometer channel. Extreme temperature structure variations at the ground (10 K heating, 10 K cooling) do not change slopes appreciably (Stork, 1984).*

ce strongly by choosing narrow spectral intervals, since the main absorption is not due to single water vapour lines, however, is due to the so-called water vapour continuum, often termed e-type absorption with reference to the vapour pressure e dependence. The origin of this absorption, either wings of distant lines or water vapour polymers, is still not known.

Because besides absorption within the atmosphere also the different emission temperatures determine $\Delta T$ we should expect a strong dependence of the water vapour contribution to $\Delta T$ on temperature structure. This is clear-
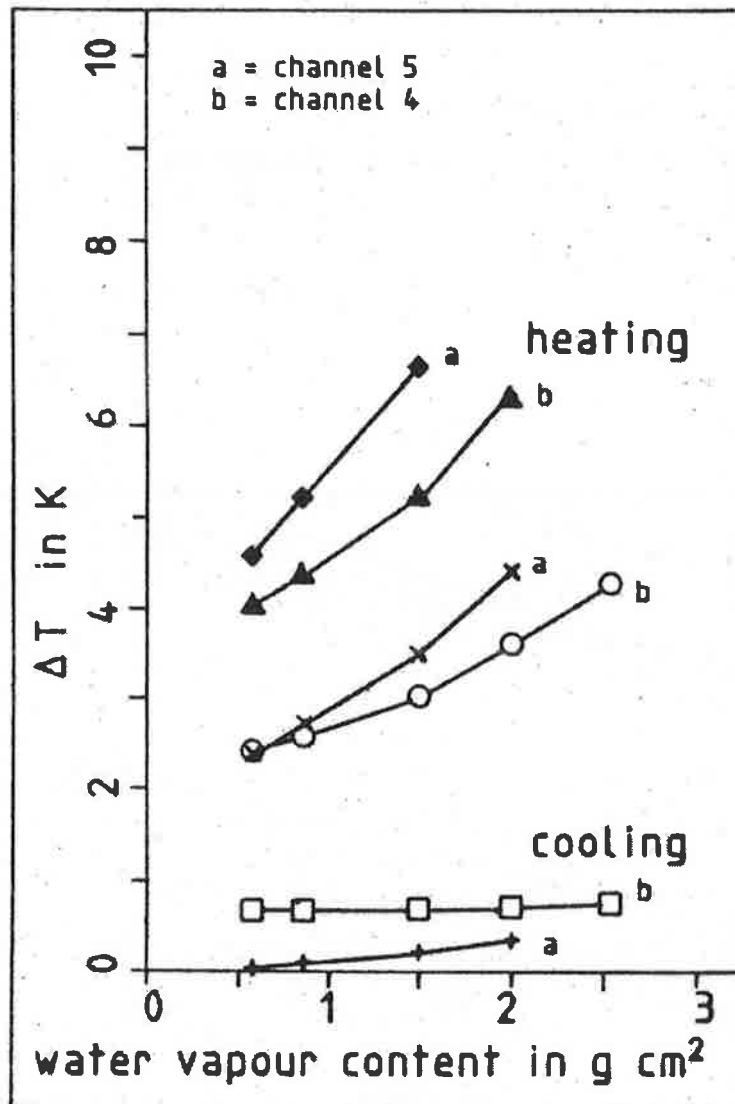


Figure 2 - Temperature correction $\Delta T$ as a function of water vapour column content for a 45 °N standard atmosphere, AVHRR channels 4 and 5, as well as surface heating and surface cooling by 10 K; nadir view; water surface emissivity $\varepsilon_\lambda$.

ly shown in Fig. 2 (modified after Stork, 1984), where $\Delta T$ for strong inversions nearly vanishes and also looses water vapour content dependence while water vapour dependence is very strong for heated surfaces (daytime dry land surface). Another fact from Fig. 2 should be stressed: even in mid-latitude atmospheres with water vapour content $< 2.5$ g m$^{-2}$ $\Delta T$ may vary between daytime and nighttime conditions by up to 8 K. Fig. 2 also indicates the advantage of a two-channel or split-window approach. The different water vapour content dependence allows an approximate calculation of $\Delta T$ without ground truth or climatology knowledge.

### 2.4.3. Temperature structure influence

The lower the temperature at which an atmospheric absorber emits (if compared to $T_s$), the higher $\Delta T$. Therefore, whenever atmospheric absorbers mask the surface, we need information on the temperature structure of the atmosphere in order to estimate the absorber's influence on remote surface temperature determination. Since water vapour content is strongly concentrated near to the ground and since it is the most important absorber in this context, the near surface temperature structure has to be investigated first.

The main results of systematic simulations of lower tropospheric temperature variations are:
— temperature inversions at the surface reduce $\Delta T$, eventually giving $\Delta T \leq 0$ for strong inversions (see also Fig. 2);
— heated surfaces lead to a strong enhancement of $\Delta T$, if compared to corresponding atmospheric temperature structure at adiabatic lapse rate;
— both above effects increase with increasing absorption, i.e. in channel 5 of the AVHRR $\Delta T < 0$ is reached earlier at increasing inversion strength;
— in many cases $\Delta T$ varies by more than 2 K between daytime and nighttime vertical temperature profiles thus rendering the application of a mean $\Delta T$ to a one channel brightness temperature $T_B$ rather useless;
— remote surface temperature determination is most difficult for daytime situations over heated land surfaces.

The second effect of temperature structure, if ordered corresponding to importance for surface temperature determination, is the low temperature in the upper troposphere and lower stratosphere. Optically thin cirrus clouds, often not detected, and stratospheric aerosol layers therefore become most important. They reduce the first term in equation (1), however, do not add at the mentioned low temperatures to the second term considerably ($B_\lambda(T) \sim T^4$ near 10 $\mu$m wavelength and thus very small at $-50°C$).

### 2.4.4. Off-nadir view

Imaging infrared radiometers like those onboard METEOSAT or NOAA-7 look onto the Earth's surface at different angles changing from pixel to pixel. Therefore $\Delta T$ has to be different for all pixels even at fixed vertical structure of the atmosphere and at fixed surface properties. While all results up to now were for nadir view, Fig. 3 demonstrates the $\Delta T$ increase also for off-nadir view.

The curves, shown for the split-window channels of NOAA-7, also account for the sphericity of the Earth. If the curves were plotted as a function of relative airmass m, they would not show a linear dependence. This is for the major part not due to the temperature decrease with height in the troposphere but due to the compensational effect of the second term in equation (3). $\Delta T \sim m^n$ with $n < 1$ leads to a doubling of $\Delta T$ (nadir) at $m > 2$, which is however, because of the sphericity of the Earth, already reached at about 50° scan angle, an angle inside the $\pm 54°$ cross-track scan of the AVHRR.

### 2.4.5. Aerosol particle effects

Aerosol particles scatter and absorb, thus it is more difficult to understand their impact on $\Delta T$ than for gases. Even as pure scatterers they would
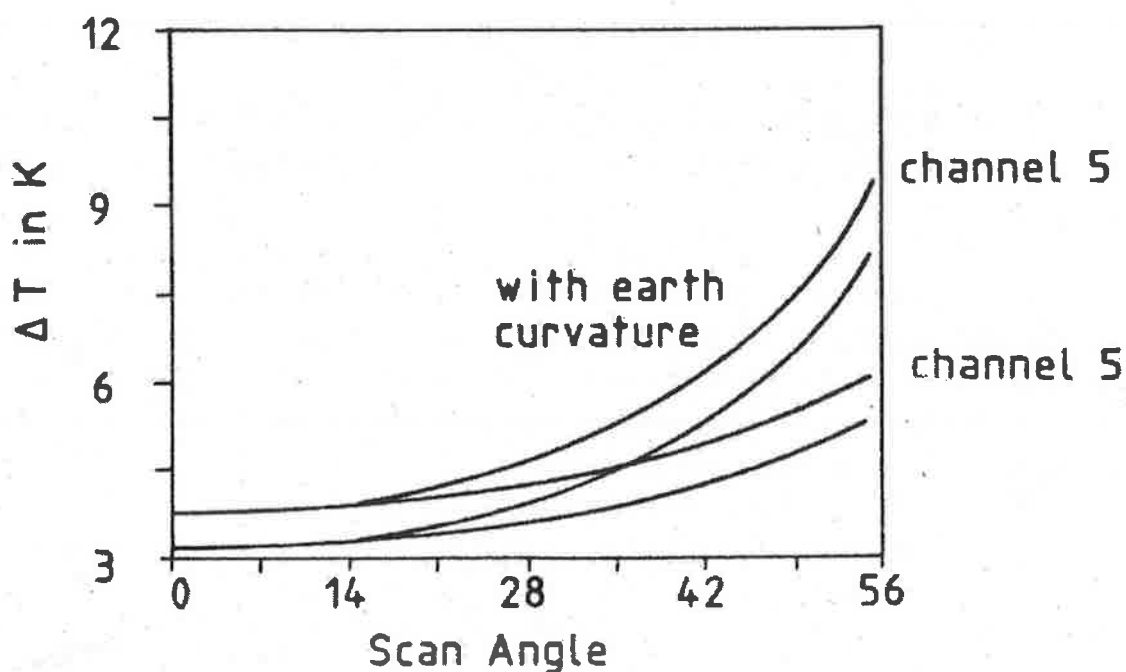


Figure 3 - $\Delta T$ as a function of the scan angle (off-nadir) for the split-window channels of the AVHRR both for a flat surface and the earth's surface.

increase $\Delta T$, because the compensating second term in equation (3) then vanishes. The typical value of total aerosol optical depth $\tau_a$ (see equation (2)) in the visible (0.55 µm wavelength normally used as a reference wavelength) is 0.2. However, $\tau_{a,0.55}$ may reach 1.0 during Saharan dust outbreaks or in metropolitan areas. At thermal infrared window wavelengths $\tau_{a,0.55} / \tau_a \approx 5$, the exact relation depending mainly on the size of the particles. Also the partitioning of extinction into scattering and absorption, thus the chemical composition plays an important role since the wavelength dependence of $\Delta T / \Delta \tau_{a,0.55}$ is not well known in the thermal infrared window. We may expect the failure of the split-window technique for aerosol effect correction and thus need additional channels for a satellite-alone retrieval of $T_S$.

Since the vertical distribution of aerosol particle number density is even more variable than that of water vapour density, the aerosol particle contribution to $\Delta T$ may vanish as for clear polar air or may be as important as water vapour in cases with high lying aerosol layers. For cases where most of the aerosol load is confined to the planetary boundary layer — the standard case — $\Delta T / \Delta \tau_{a,0.55} \simeq 5$ K per unit optical depth; i.e. typically 0.5 K have to be added to satellite brightness temperatures in order to compensate for the aerosol effect. The exact value of $\Delta T / \Delta \tau_{a,0.55}$ additionally depends rather strongly on relative humidity and water vapour column content.

### 2.4.6. Optically thin clouds

Any surface temperature algorithm applied so far has to rely on a cloud detection procedure applied before the temperature algorithm. Because of a frequent failure of cloud detection algorithms for optically thin or subpixel sized clouds the possible influence of thin cirrus clouds on brightness temperatures is shown as an example. Fig. 4 from Manschke (1985) also includes aerosol effects. It is clearly seen that:

— the difference $\Delta T_B = T_B(3) - T_B(4)$ of channels 3 at 3.7 µm and 4 at 11 µm of the AVHRR is well suited for a cloud detection;

— aerosol effects at a horizontal visibility change from 23 to 5 km are smaller than those for 0.05 optical depth of a cirrus at 10 km height;

— aerosol effects also have more impact on $T_B(3) - T_B(4)$ than on $T_B(4) - T_B(5)$;

— differences among atmospheres dominate $\Delta T_B$ for $\tau_{cirrus} \leq 0.1$ thus offering $T_S$ determination through thin cirrus as shown by Manschke (1985) for water surfaces.

Different procedures to detect also thin and subpixel sized clouds will be presented in section 3.5.

### 2.4.7. Other influences

The thermal infrared window from 10-13 μm as well as other smaller thermal infrared windows are not free of absorption by other gases than water vapour. For well mixed gases like carbon dioxide ($CO_2$), methane ($CH_4$) and nitrous oxide ($N_2O$) the influence has been taken into account for the simulations presented. They also pose no severe problems when applying $T_S$ retrieval algorithms to satellite data. Depending on the satellite radiometer channel also ozone may be important for the exact $\Delta T$ (Grassl and Keopke, 1980).

## 3. Algorithms

It is now common practice to call an equation coupling satellite radiances and atmospheric parameters via an empirical or semi-empirical though simple
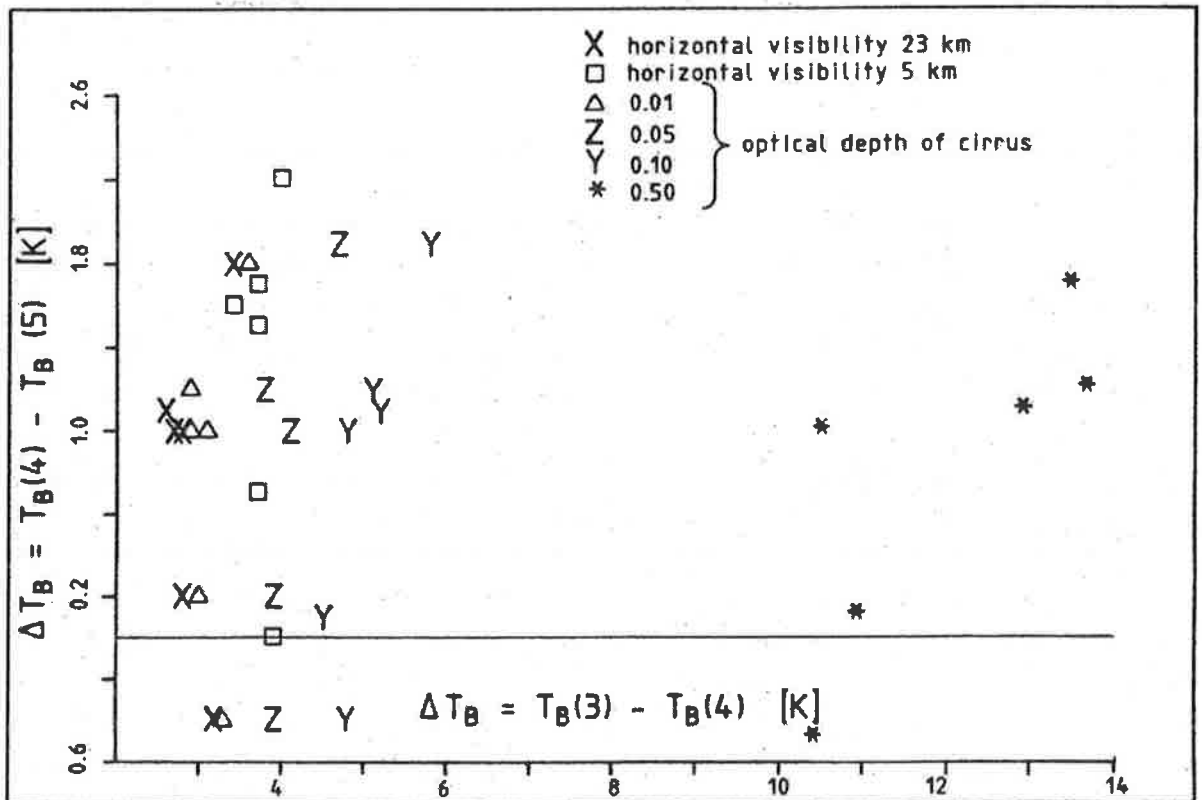


Figure 4 - Brightness temperature differences $\Delta T_B = T_B(3) - T_B(4)$ versus $\Delta T_B = T_B(4) - T_B(5)$ for 6 atmospheres (45 °N summer, autumn, winter; subarctic summer and winter tropics 10 °N) and at 6 cirrus or aerosol disturbances as indicates.

relation an algorithm. Despite a possible success when «playing» with brightness temperatures or their differences during the search for a retrieval procedure or an algorithm one should normally start with the basic equation, simplify it and then adjust some parameters by validating remote measurements with in-situ data whenever possible. This way will be chosen for the multichannel approach, however, at first one-channel surface temperature estimation will be touched.


## 3.1 $T_s$ from a single channel

From the variability of the temperature correction $\Delta T$, shown in section 2.4, follows that surface temperature $T_S$ from a single channel will be least accurate over heated land surfaces at high relative humidity and high level turbidity, if only climatological corrections $\Delta T$ are applied to the satellite data. Under these circumstances and for the outer parts of the swath $\Delta T \simeq + 10$ K is not rare.

On the other hand for a nearby lake in spring as shown by McClain (1986) $\Delta T \leq 0$ K may be correct. Thus the satellite brightness temperature may often smoothes horizontal surface temperature differences. How should one then proceed, if only one channel is available? The answer is:

Use as much additional information as is available. This additional information may be:
— radiosonde data;
— short term temperature profile forecasts;
— routine air temperature (2 m height) observations;
— bulk temperature observations in lakes and rivers;
— physical models of relative near surface temperature profiles as a function of season and daytime;
— calibration by a multichannel satellite radiometer (for example AVHRR for METEOSAT as shown by Singh *et al.*, 1985).

In this context the impact of the emissivity difference $\Delta \varepsilon_\lambda = 1 - \varepsilon_\lambda$ over land is often exaggerated, since over vegetated surfaces it is small; even if for a tiny surface element (dry leaf) $\Delta \varepsilon_\lambda$ may reach 0.1, the roughness of all vegetation causes the mean emission of a satellite pixel to approach the blackbody emissivity: a wheat field is composed of many «black» holes. However, this discussion leads us to the difficulty of defining mean surface temperature of rough surfaces. While we have no difficulties for smooth water surfaces (it is the skin temperature with radiation originating from the uppermost micrometers), we may still call it the surface temperature of a forest, although

all portions of trees, the grass and the ground below contribute in varying amounts.

$\Delta T$ is more strongly influenced by heating or cooling of surfaces relative to the atmospheric temperature above the surface layer than by the emissivity deficit $\Delta \varepsilon_\lambda$.

### 3.2 $T_s$ from at least two channels

Firstly, by simplifying equation (3) the basic two-channel or split-window algorithm will be derived, following McMillin (1975). Neglecting the third term in equation (3), the contribution by reflecting atmospheric emission, thus setting $\varepsilon_\lambda = 1$ and applying the mean value theorem we get

$$I_\lambda^+ = B_\lambda \; (T_s) \; e^{-\overset{*}{\lambda}} + B_\lambda \; (\bar{T}) \; (1 - e^{-\overset{*}{\lambda}}) \tag{11}$$

with $\bar{B}_\lambda(\bar{T})$ = mean spectral radiance of the atmosphere, Planck's function at an appropriate temperature $\bar{T}$ for a given transmission

$$t = e^{-\overset{*}{\lambda}}$$

For two channels, i.e. two different wavelength intervals, the spectral dependence of upward radiance $I_\lambda^+$ and the source function, Planck's function $B_\lambda(T)$, have to be introduced, here by a Taylor expansion truncated after the first expansion term

$$B(\lambda_r, T) \simeq B_\lambda(T) + \frac{\partial B_\lambda(T)}{\partial \lambda}(\lambda_r - \lambda) \qquad \text{and} \qquad \tag{12a}$$

$$I^+(\lambda_r) \simeq I_\lambda^+ + \frac{\partial I_\lambda^+}{\partial \lambda}(\lambda_r - \lambda) \tag{12b}$$

where $\lambda_r$ is a reference wavelength within the 10-13 µm window. Since $T_s$, $T$ and $T_I$ (reached by inversion of $I_\lambda^+$) are close together for the 10-13 µm range and thus will not change appreciably with $\lambda$, we put

$$\frac{\partial I_\lambda^+}{\partial \lambda} \simeq \frac{\partial B_\lambda(\bar{T})}{\partial \lambda} \simeq \frac{\partial B_\lambda(T_s)}{\partial \lambda} \simeq \frac{\partial B_\lambda(T_I)}{\partial \lambda} \tag{13}$$

Equation (11) for any radiometer channel wavelength interval $\Delta\lambda_i$ within the 10-13 μm range then is simplified into equation (11) into 12b; 12a into the result

$$I^+_{\Delta\lambda_i} = B_{\lambda_r}(T_s)\, e^{-\tau^*_{\lambda_i}} + \bar{B}_{\lambda_r}(\bar{T})\,(1 - e^{-\tau^*_{\lambda_i}}) \tag{14}$$

Writing equation (14) for two channels using $B_{\lambda_{1r}}(\bar{T}) \cong B_{\lambda_{2r}}(\bar{T})$, which is proven by radiative transfer calculations, subsequent substraction and resolving for $B_{\lambda_r}(T_s)$ gives

$$B_{\lambda_r}(T_s) = I^+_{\lambda_{1r}} + \frac{1 - e^{-\tau^*_{\lambda_1}}}{e^{-\tau^*_{\lambda_1}} - e^{-\tau^*_{\lambda_2}}}\,(I^+_{\lambda_{1r}} - I^+_{\lambda_{2r}}) \tag{15}$$

$$= I^+_1 + \gamma\,(I^+_1 - I^+_2)$$

If this equation is converted into an equation for brightness temperatures $T_B$ (see equation (5)) the basic version of the split-window algorithm is found

$$T_s = T_B(1) + b\, T_B(1) - T_B(2) + a \tag{16}$$

where the constant a accounts for errors due to the simplifications (equations (11), (12), (13) and $B_{\lambda_{1r}} = B_{\lambda_{2r}}$) used to derive equation (16) from equation (3).

## 3.3 Achievements of the split-window algorithm over water

The algorithm (16) has been used primarily for sea surface temperature determination and numerous coefficients have been derived by different groups (examples are Strong and McClain, 1984; Llewellyn-Jones et al., 1984; Schlüssel et al., 1987). The differences in coefficients a and b mainly stem from the set of atmospheres and in-situ data used, the accuracy and the quantity with which a comparison has been made, for instance bulk or skin temperature measured from a buoy or from a ship. It has also been shown that a regional algorithm is superior to a global, if only two channels are available (Llewellyn-Jones et al., 1984). The accuracies achieved by the two NOAA satellites with a split-window (NOAA 7 and NOAA 9) are best documented by showing the increased accuracy during the buoy-satellite match-
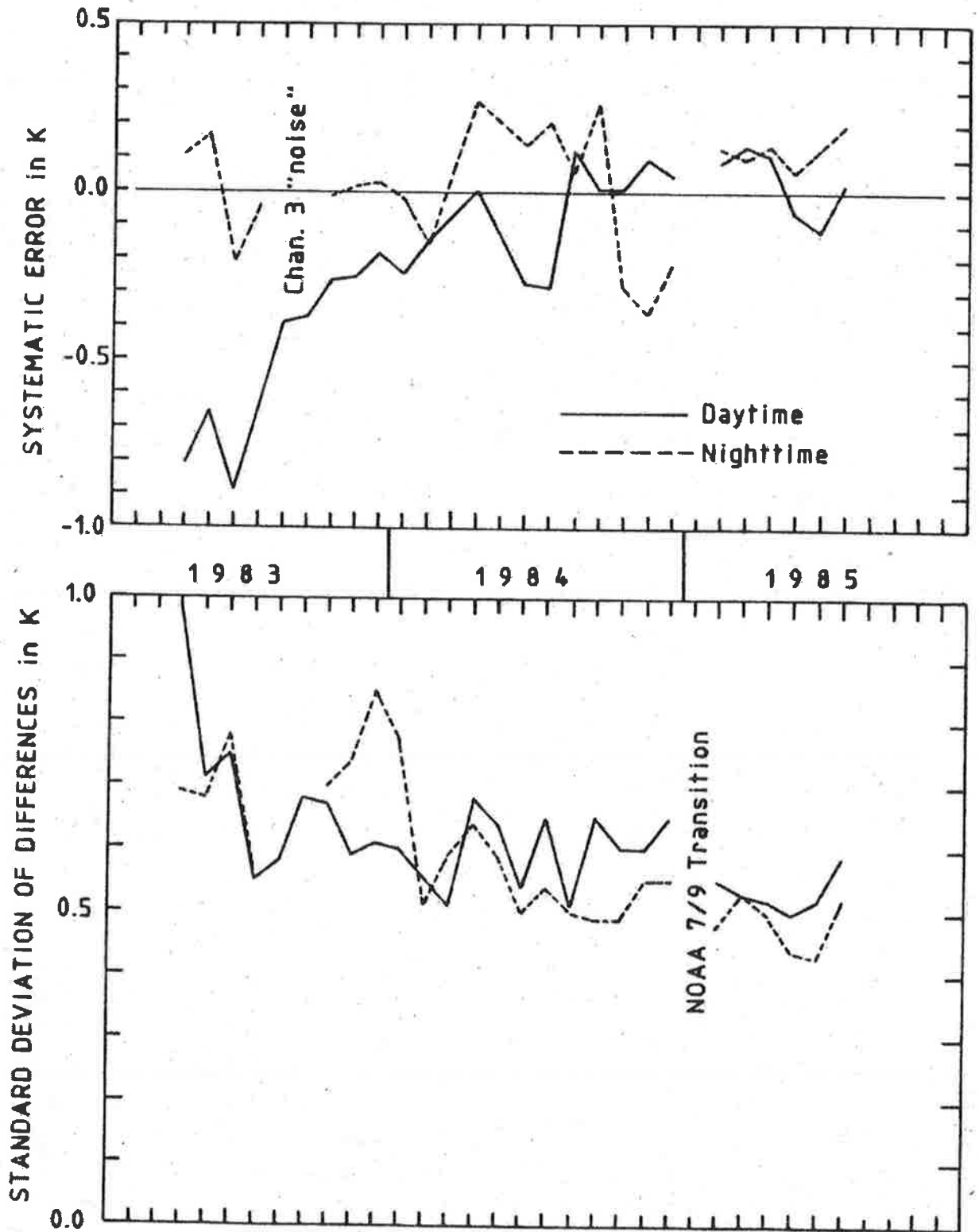
Figure 5 - *Systematic error and standard deviation monthly means between satellite derived and buoy bulk temperatures as a function of time for the split-window technique. Nighttime temperatures use also channel 3 and thus a modified algorithm.*

ups in Fig 5 and the accuracies after classification into daytime, nighttime and humidity intervals in Table 2 (taken from WCP-110, 1986).

TABLE 2a - *February-August, 1985: matchup statistics for day and night and for different areas*

| Region | Day | | | Night | | |
|---|---|---|---|---|---|---|
| | No. | Bias | RMSD | No. | Bias | RMSD |
| World | 1625 | +0.01 | 0.55 | 1042 | +0.12 | 0.48 |
| W. Trop. Pac. | 189 | −0.02 | 0.47 | 102 | +0.22 | 0.40 |
| E. Trop. Pac. | 433 | −0.15 | 0.55 | 290 | +0.08 | 0.41 |
| Trop. Atl. | 424 | +0.08 | 0.51 | 277 | +0.12 | 0.51 |
| Trop. Ind. | 277 | −0.03 | 0.50 | 163 | +0.11 | 0.46 |
| N. Atl. & Pac. | 208 | +0.18 | 0.60 | 115 | +0.18 | 0.54 |
| N. Pac. | 112 | +0.25 | 0.65 | 74 | +0.16 | 0.59 |
| N. Atl. | 96 | +0.10 | 0.53 | 41 | +0.23 | 0.46 |
| Southern Ocean | 139 | +0.08 | 0.63 | 113 | +0.11 | 0.44 |

TABLE 2b - *February-August, 1985: matchup statistics by moisture class indicated by the brightness temperature difference classes*

| Moisture (Tropical Oceans) | Day | | | Night | | |
|---|---|---|---|---|---|---|
| | No. | Bias | RMSD | No. | Bias | RMSD |
| $0° < T_4 - T_5 < 1°$ | 500 | −0.08 | 0.47 | 218 | +0.16 | 0.47 |
| $1° < T_4 - T_5 < 2°$ | 694 | +0.00 | 0.56 | 553 | +0.09 | 0.46 |
| $2° < T_4 - T_5 < 3°$ | 69 | −0.01 | 0.61 | 38 | −0.01 | 0.52 |

## 3.4 Algorithms over land?

Knowing the main result for water surfaces, namely a temperature nearly free of systematic errors and with only 0.5 K rms error, we ask whether the split-window algorithms may be applied to land surfaces. The answer is no, since the following facts have to be taken into account:

— spectral emissivity changes from one surface type to the next, causing a $\Delta T_B$ of the same magnitude as humidity (see Table 2b) and thus leading to a false $\Delta T$;

— cloud detection during daytime is exceptionally difficult over bright surfaces like snow or sand dunes;

— strong near surface heating or cooling is only partly accounted for by two spectral channels.

My proposal for a procedure for land surface temperature determination from two or more satellite brightness temperatures therefore was:

1) determine cloud-free parts;

2) use the split-window algorithm (16) over water surfaces within the area envisaged;

3) inter- and extrapolate the «water surface» atmospheric correction;

4) derive an additional correction from the brightness temperature difference between water surfaces and a land surface pixel for the channels available.

5) choose after adding the second correction the highest temperature to reach a good estimate of surface temperature.

## 3.5 Application of the proposed procedure to ALPEX SOP satellite data

During one of the special observing periods (SOP) within the ALPEX (Alpex Experiment) rather cloudfree satellite data during day — and night-time could be acquired on 25th and 26th March 1982. For this time the procedure outlined above has been applied to NOAA 7 data by Stork (1984). Since the images cover a big part of the Alps this has been a hard test as far as cloud clearing and interpolation is concerned.

Step 1. Cloud clearing

Four different procedures have been applied simultaneously to daytime images. They are displayed in Table 3.

Nighttime cloud clearing, rather easy over water, as shown by Olesen and Grassl (1985), is more difficult over land. Therefore no table similar to Table 3 can be shown.

TABLE 3 - *Cloud clearing thresholds (cloudy if above this threshold)*[*]

| Water surfaces | Snowfree land surfaces |
|---|---|
| Channel 1: $A_s \geq 0.15$[**] | $A_s > 0.15$ |
| Channel 2: $A_s \geq 0.15$ | $A_s > 0.24$ |
| $T_B(3) - T_B(4) > 3$ K | $T_B(3) - T_B(4) > 5$ K |
| $T_B(4) - T_B(5) > 1.7$ K | $T_B(4) - T_B(5) > 1.9$ K |

[*] All thresholds have been chosen interactively at an image processing system.

[**] $A_s$ = albedo.

Step 2. Surface temperature over water surfaces

For midlatitude atmospheres and the NOAA 7 satellite the split-window algorithm (16) for water surfaces is, following Jürgensen (1984)

$$T_s = 3.345 \, T_B(4) - 2.363 \, T_B(5) + 5.74 \, K \tag{17}$$

This algorithm has been applied to all big lakes within the scene and to the Adriatic Sea.

Step 3. Inter- and extrapolation

Before an interpolation the atmospheric corrections over water ranging from 2 to 3 K for all big lakes and the Adriatic Sea were spatially averaged. Thus the noise in single $\Delta T$'s due to the 0.12 K noise equivalent $\Delta T$ (NE$\Delta T$) of the satellite radiometer was strongly suppressed. The rather small number of lakes does not allow a polynomial of higher order to be fit to the water surface $\Delta T$'s. Therefore only a first and second order polynomial were chosen. Even the second order polynomial led to strong errors within the extrapolation area. Whenever extrapolation is necessary we have chosen as atmospheric correction $\Delta T$ for the image coordinates x,y and for channel i

$$\Delta T_i(x,y) = a_{1_i} \, x + a_{2_i} \, y + a_{3_i} \tag{18}$$

leading to a first approximation of surface temperature

$$T_{s_1}(x,y) = T_B(i) + \Delta T_i(x,y) \tag{19}$$

$T_{s_1}$ still contains errors due to the near surface heating or cooling as well as emissivity changes.

Step 4. Additional correction derived from the water-land contrast

As shown in section 2.4 the heating or cooling of land surfaces increases or decreases the correction $\Delta T$. For a midlatitude atmosphere (45° N) the additional correction may reach 3 K for a +20 K change in surface temperature. From model simulations found for channels 4 and 5

$$\begin{aligned} \Delta T_4' &= 0.14 \, \Delta T_{s_1}(4) \\ \Delta T_5' &= 0.22 \, \Delta T_{s_1}(5) \end{aligned} \tag{20}$$

These relations also hold for cooling, i.e. for negative temperature differences $\Delta T_{s_1}$ if $\Delta T_{s_1}$ is the difference between $T_{s_1}$ and the interpolated water surface temperature. After this correction the second approximation for $T_s$ is reached

$$T_{s_2}(i) = T_B(i) + \Delta T_i(x,y) + \Delta T_i' \tag{21}$$

$\Delta T_4'$ as well as both corrections (19) and (20.) are shown in Fig. 6.

Step 5. Correction of emissivity changes

The effects of unknown surface emissivity and thus of unknown spectral dependence can only be removed partially. After applying corrections (19) and (21) to channel 4 and 5 one should choose the channel with higher temperature, since this channel should be the channel nearer to a blackbody emission. Choosing the higher temperature we arrive at $T_s$, the quantity desired. However, whenever the difference of $T_s$ between both channels surmounts 1 K, pointing to $\Delta\varepsilon_\lambda > 2\%$ we discard this value and classify the pixel as cloud contaminated.

$T_s$ from Figs. 7 and 8a,b contains a wealth of information for climatologists.

### 3.6 Error analysis

The following error sources have to be discussed:
— conversion from counts to brightness temperatures;
— split-window algorithm for water surfaces (equation (17));
— interpolation errors (equation (18));
— water-land differences (equation (20));
— remaining emissivity difference.

The conversion from counts with a 10 bit resolution to brightness temperature is according to Singh (1984) accurate to 0.01 K and thus errors are negligibly small. The radiometric noise expressed by the noise equivalent temperature difference (NE$\Delta$T = 0.12 K for channels 4 and 5 of AVHRR and for the 270 to 300 K range) is easily suppressed by spatial averaging. The split-window algorithm combining errors due to changing atmospheric structure not resolved and the NE$\Delta$T after spatial averaging is affected by a 0.5 K rms error (see Table 2). If — as done here — $T_s$ is determined on a pixel by pixel basis the combination leads to a slightly higher standard error for water surface temperature determination.

The interpolation error strongly depends on the number of water surfaces found in a scene. For 23 lakes in the chosen scene and the first order polynomial (18) the error of the atmospheric correction $\Delta T$ for water surfaces reaches 0.6 and 0.85 K for channel 4 and 5, respectively.

The adoption of this interpolated correction for synthetic water surfaces, $\Delta T_i$ (x,y), as a first approximation (equation (19)) for land surface temperature, enhances the rms error from 0.51 K for lakes to 0.8 K over land if choosing the more transparent channel 4. This error would increase to 1.0 K for channel 5. One should, however, be aware of the large systematic errors

*Figure 6 - a) $\Delta T'_4$ for the daytime overpass in steps of 0.5 K indicated by different colours (see scale below image); b) $\Delta T_4(x,y) + \Delta T'_4$ for the same scene.*
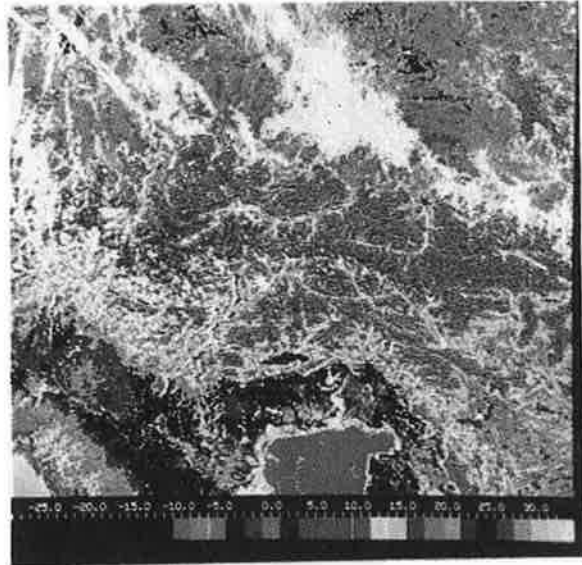


*Figure 7 - Surface temperature for the daytime overpass in steps of 2 K (25 March 1982, early afternoon); clouds are white.*
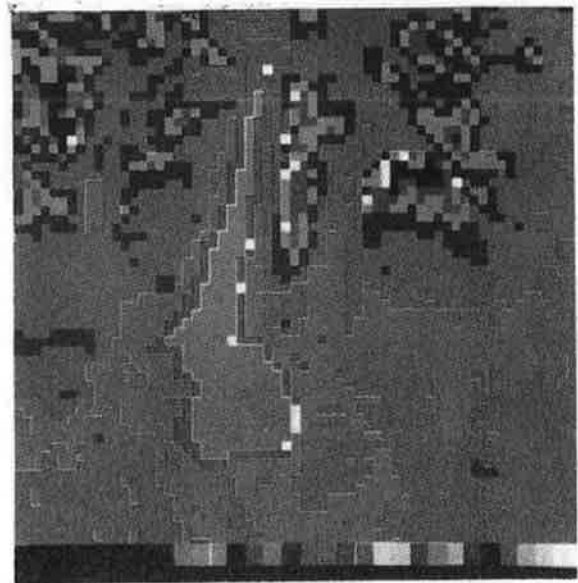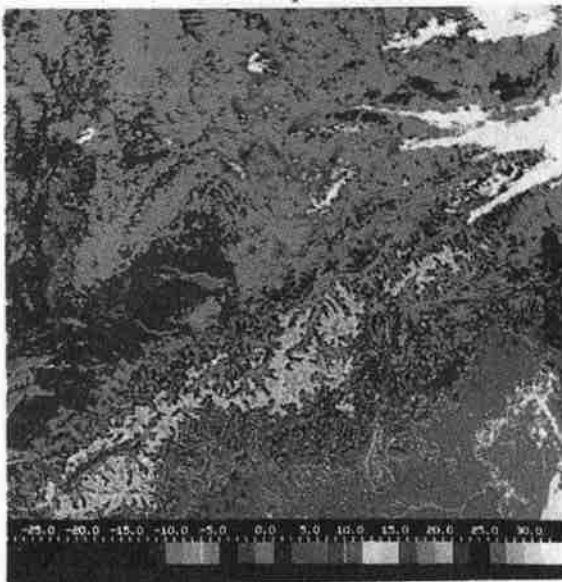




*Figure 8 - Surface temperature for the nighttime overpass in steps of 2 k (26 March 1982, early morning): a) for the full image; b) zoom around Lago di Garda, Northern Italy.*

left because of heated or cooled surfaces and emissivity changes. These systematic errors are reduced by steps 4 and 5 (section 3.4). On the other hand step 4 increases the rms error to 0.9 K for channel 4 and 1.1 K for channel 5.

The discussion of errors due to surface emissivity changes is more difficult. Since $\Delta\varepsilon_{\Delta\lambda} = 0.02$ is the upper limit for differences within the 10-13 μm window for smooth rock surfaces and since this would cause a systematic underestimation of $T_s$ by about 1 K, we expect over vegetated surfaces with $\varepsilon_{\Delta\lambda} > 0.95$ and $\Delta\varepsilon_{\Delta\lambda} < 0.02$ an additional systematic error $\leq 1$ K, which, however, is reduced by step 5 where the higher temperature of both channels is chosen.

An accuracy of 1-2 K for $T_s$ of land surfaces is at least for daytime situations, where the atmospheric masking may reach 10 K, a step forward.

A verification of the approach described is only possible by radiometric measurements from masts and air planes. This has been shown to be successful for ocean surfaces (Schlüssel et al., 1987) by measurements from ship, where also by a combination of satellite radiometers a 0.3 K rms error has been reached.

## 3.7 The daily temperature amplitude

The climatologist is sometimes even more interested in daily temperature amplitudes $\Delta T_D$ than in $T_s$, because they are an indication for evaporation and thus help in remotely sensing latent heat fluxes. Already before an application of the approach discussed above for remote land surface temperature determination we had derived $\Delta T_D$ for the ALPEX scenes used so far (Grassl et al., 1985).

In the inner Inn Valley, at Schwaz in Tirol, we could show by using ground observations and radio soundings that $\Delta T_D$ (Fig. 9) is accurate to at least 2 K without any atmospheric correction in a valley wind system. The time of the NOAA7 satellite overpasses at approximately 2.30 a.m. and p.m. guarantees observations at the daily temperature maximum and — best for valleys with a valley wind system — very near to the temperature minimum. Under calm conditions, however, with strong heating during daytime the procedure outlined in section 3.4 has to be applied especially for the daytime overpass (see Fig. 2).

## 3.8 Further improvements

Recently Schlüssel (1987) has demonstrated that a combination of two radiometers on board the NOAA satellite series, namely the AVHRR and the
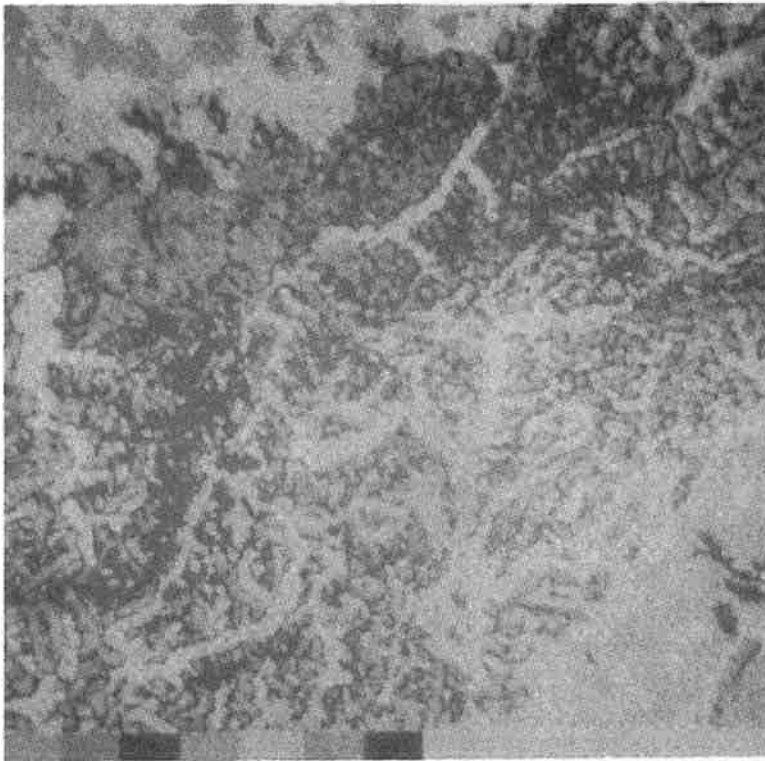
*Figure 9 - Daily temperature amplitude for parts of the Alps derived solely from brightness temperature diffe-rences between 25 March, ~2.30 p.m. and 26 March, ~2.30 a.m.*

HIRS (High Resolution Infrared Sounder) improves not only temperature and humidity profiles but also surface temperature over water surfaces. A 0.3 K rms error was found during a verification cruise in the North-East Atlantic for some case studies. The additional information comes from a 6.3 μm band water vapour channel whose weighting function peaks in the lowest tropo-sphere and from three 15 μm-$CO_2$ channels peaking in the lower troposphere and at the ground. Especially the algorithm over big lakes and marginal seas would gain in accuracy by introducing the combined algorithm which also accounts for changing coefficients at different viewing angles. However, the latter improvement is also possible for the split-window algorithm (16). De-spite the higher accuracy demonstrated for marginal seas there are still ex-treme conditions (McClain, 1986) in spring over the American big lakes where the improved algorithm failed. Therefore it might be dangerous to take 0.5 K rms error for granted over lakes as done in section 3.6.

# References

GRASSL H. and KOEPKE P., 1981. Corrections for atmospheric attenuation and surface reflectivity in satellite-borne SST measurements. In: *Oceanography from space,* Plenum Press, 97-107.

GRASSL H., STORK T. and RÜSTEN C, 1985. Daily temperature amplitude at the surface from NOAA-7. *Zbornik Meteoroloskih i Hydroloskih Radova,* 11, 36-39.

JÜRGENSEN A., 1984. Bestimmung des Wasserdampfgehaltes der Atmosphäre über dem Ozean aus Satellitendaten. Diploma Thesis, University of Kiel, FRG.

LLEWELLYN-JONES S.T., MINNETT P.J., SAUNDERS R.W. and ZAVODY A.M., 1984. Satellite multichannel infrared measurements of sea surface temperature of the North-East Atlantic ocean using AVHRR/2. *Quart.J. R. Met. Soc.,* 110, 613-631.

MANSCHKE A., 1985. Einfluss dünner Cirren auf den Strahlungshaushalt. Diploma Thesis, University of Kiel, FRG.

McCLAIN P., 1986. Private communication.

McMILLIN L.M., 1975. Estimation of sea surface temperatures from two infrared window measurements with different absorption. *J. Geophys. Res.,* 80, 5113-5117.

OLESEN F.-S. and GRASSL H., 1985. Cloud detection and classification over oceans at night with NOAA-7. *Int. J. Rem. Sens.,* 6, 1435-1444.

SCHLÜSSEL P., 1987. Infrarotfernerkundung von Oberflächentemperaturen sowie atmosphärischen Temperatur- und Wasserdampfstrukturen. Ph. D. Thesis, University of Kiel. Berichte aus dem Inst. f. Meereskunde, Nr. 161, 116 pages.

SCHLÜSSEL P., SHIN H.-Y., EMERY W. J. and GRASSL H., 1987. Comparison of satellite derived sea surface temperatures with in-situ skin measurements. *J. Geophys. Res.,* March issue.

SINGH S.M., 1984. Removal of atmospheric effects on a pixel basis from the thermal infrared data from instruments on satellites. The Advanced Very High Resolution Radiometer (AVHRR). *Int. J. Rem. Sens.,* 5, 161-183.

STORK T., 1985. Bestimmung der Oberflächentemperatur über Land aus Satellitendaten. Diploma Thesis, University of Kiel, FRG.

STRONG A.E. and McCLAIN E.P., 1984. Improved ocean surface temperatures from space: comparison with drifting buoys. *Bull. Am. Met. Soc.,* 65 , 138-141.

WCP-110, 1986. Satellite-derived sea surface temperatures for global climate applications. Report of the COSPAR. International Workshop, Camp Springs, Maryland, USA, 28-31 May, 1985; World Climate Programme Series, WMO, Geneva.

## Determinazione della temperatura della superficie terrestre mediante dati forniti dal satellite

In questa relazione viene illustrata brevemente la teoria del rilevamento a distanza mediante le onde elettromagnetiche nella parte visibile ed infrarossa dello spettro e vengono presi in esame i parametri della superficie, le caratteristiche dei gas e delle particelle di aerosol che influiscono sulla misurazione a distanza della temperatura di superficie. Inoltre si riportano gli algoritmi impiegati per la misurazione a distanza di tipo «stand-alone» della temperatura di superficie e si esaminano varie applicazioni dei diversi algoritmi, fra le quali anche la determinazione dell'escursione termica nell'arco della giornata.